Article published online: 2022-06-30

Discovery of Indole-Containing Benzamide Derivatives as HDAC1 Inhibitors with *In Vitro* and *In Vivo* Antitumor Activities

Xiu Gu[1,2] Xin-Yan Peng[2] Hao Zhang[2,3] Bo Han[2] Min-Ru Jiao[2] Qiu-Shi Chen[1] Qing-Wei Zhang[2*]

[1] School of Chemistry and Chemical Engineering, Shanghai University of Engineering Science, Shanghai, People's Republic of China
[2] Novel Technology Center of Pharmaceutical Chemistry, Shanghai Institute of Pharmaceutical Industry Co., Ltd., China State Institute of Pharmaceutical Industry, Shanghai, People's Republic of China
[3] School of Pharmacy, Fudan University, Shanghai, People's Republic of China

Address for correspondence Qing-Wei Zhang, PhD, Novel Technology Center of Pharmaceutical Chemistry, Shanghai Institute of Pharmaceutical Industry Co., Ltd., 285 Gebaini Road, Shanghai 201203, People's Republic of China (e-mail: sipiqingwei@163.com).

Pharmaceut Fronts 2022;4:e61–e70.

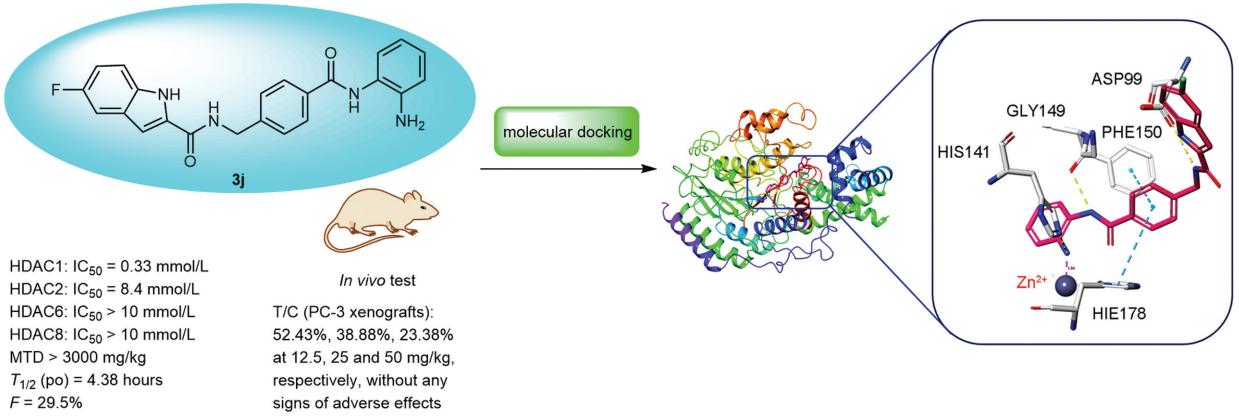

Abstract

Targeting histone deacetylases (HDACs) has become an important focus in cancer inhibition. The pharmacophore of HDAC inhibitors (HDACis) reported so far is composed of three parts: a zinc-binding group (ZBG), a hydrophobic cavity-binding linker, and a surface-recognition cap interacting with HDAC surface located at the rim of active site cavity. This study aims to discover novel HDAC1 inhibitors with potent antitumor activities through modifying the cap and ZBG based on the structures of two marketed oral HDACis: chidamide and entinostat (MS-275). In this work, a series of benzamide derivatives were designed, synthesized, and evaluated for their antitumor activity. The structures of novel compounds were confirmed by ^{1}H NMR (nuclear magnetic resonance) and ESI-MS (electrospray ionization mass spectrometry), and all target compounds were tested in both HDAC1 enzymatic inhibitory activity and cellular

Keywords
- chidamide
- benzamide
- HDAC1 inhibitors
- synthesis
- antitumor

received
December 21, 2021
accepted
April 21, 2022

DOI https://doi.org/10.1055/s-0042-1749373.
ISSN 2628-5088.

Georg Thieme Verlag KG, Rüdigerstraße 14, 70469 Stuttgart, Germany

antiproliferative activity. Our data showed that the potent compound **3j** exhibited good HDAC1 enzyme inhibitory activity and high antitumor cell proliferation activity against a selected set of cancer cells (PC-3, HCT-116, HUT-78, Jurkat E6–1, A549, Colo205, and MCF-7 cells) with no observed effects on human normal cells. In particular, compound **3j** inhibited HDAC1 over the other tested HDAC isoforms (HDAC2, HDAC6, and HDAC8). Encouraged by this, the safety characteristics, molecular docking, preliminary pharmacokinetic characteristics, and antitumor effect *in vivo* of compound **3j** were further investigated. Our data showed that compound **3j** demonstrated acceptable safety profiles and favorable oral pharmacokinetic properties. Moreover, compound **3j** could bind well with HDAC1 and showed significant antitumor activity in a PC-3 tumor xenograft model *in vivo*, though not as potent as positive control entinostat (MS-275). In summary, **3j** might have therapeutic potential for the treatment of human cancers.

Introduction

Epigenetics is a study of a heritable change in gene function that culminates in a phenotypic change without altering DNA sequences.[1] It plays an important role in cellular and molecular regulatory processes.[2,3] Epigenetic defects can lead to altered gene function and malignant cellular transformation and have been linked to the progression of several diseases, such as cancer.[4,5] The reversible acetylation of histones, which is controlled by histone acetyltransferases and histone deacetylases (HDACs), is an important epigenetic modification implicated in cell proliferation and has been identified as a valuable target for anticancer drug.[6,7] HDACs comprise a family of 18 genes, which are grouped into "classical HDACs" (Zn^{2+} for classes I, II, and IV) and sirtuins (NAD^{+} for class III) based on their catalytic mechanisms.[8] While the biological functions of many HDAC subtypes are still being defined, there is compelling evidence that class I HDACs (HDAC1, 2, 3, 8) are overexpressed in human cancers and therefore are viable targets for cancer therapeutics.[9–12]

Currently, four HDAC inhibitors (HDACis), including vorinostat (SAHA), belinostat, panobinostat, and romidepsin, have been approved by Food and Drug Administration for the treatment of refractory or relapsed cutaneous and peripheral T cell lymphomas, or multiple myeloma (►**Fig. 1**).[13] Unlike most "pan-HDACis" having an hydroxamic acid zinc-binding motif, HDACis containing an ortho-aminophenyl benzamide selectively inhibit HDACs 1–3. Specifically, entinostat (MS-275),[14] mocetinostat (MGCD0103), and chidamide (CS055) not only maintain

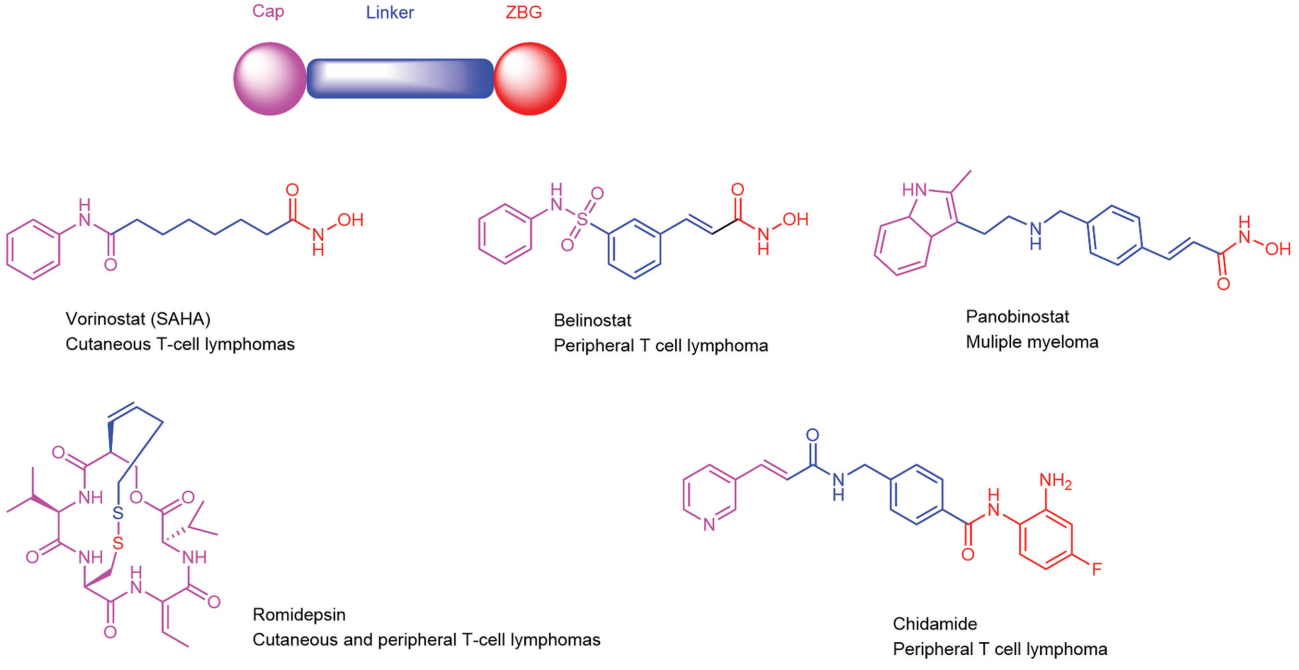

Fig. 1 Currently approved HDACis for cancer treatment in clinical practice (chidamide was approved in China) and their representative pharmacophore model: cap, linker, and ZBG. HDACis, histone deacetylases inhibitors; ZBG, zinc-binding group.

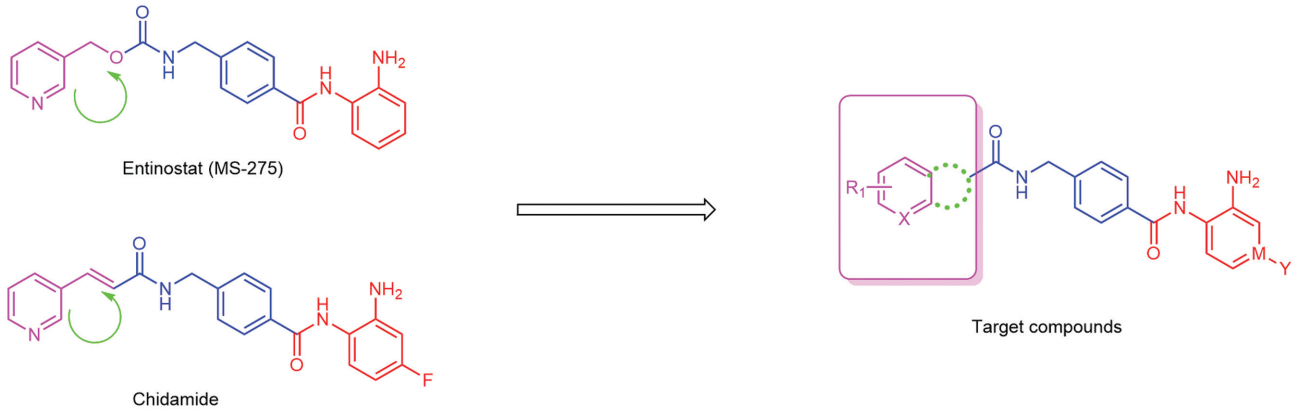

Fig. 2 The structures of entinostat, chidamide, and our design strategy of target compounds.

potent enzymatic and cellular inhibition of HDACs activity *in vitro* but also display remarkable improvements in pharmacokinetic (PK) properties and antitumor efficacy *in vivo*. Besides, chidamide (**4**) was the first orally available benzamide HDACi developed and approved in China for peripheral T cell lymphoma treatment.[15]

The chemical structures of most HDACis reported so far can be divided into three functional parts,[16–18] consisting of a zinc-binding group (ZBG), a hydrophobic cavity-binding linker, and a surface-recognition cap interacting with HDAC surface located at the rim of active site cavity. The structural similarity of the existing class of benzamide HDACis suggested that rational isosteric modification of the surface-recognition domain or ZBG is feasible. The discovery of novel benzamide HDACis with high anticancer potency and good safety profiles is still a major activity of basic and clinical research.[19–21]

Inspired by our identification of a new HDACi for cancer treatment,[7,22] cap and ZBG were modified based on the structures of chidamide and entinostat (MS-275) (►**Fig. 2**), and a series of new benzamide HDAC1 inhibitors were designed and synthesized. Then, preliminary structure–activity relationship (SAR) analysis, antiproliferative activity, safety, and *in vivo* efficacy of these potent HDACis were further discussed.

Results and Discussion

The synthetic routes of target compounds are shown in **Scheme 1**. First, different fragments, such as quinoline, naphthalene, indole, and thiophene, were inserted into the cap region to synthesize compounds **3a–3 g**. After screening for HDAC1 inhibition, it was determined that the indole fragment in the cap region had the best activity. Then, compounds **3h–3o** were synthesized with different substituents inserting into the 5 position of indole and the *o*-aminophenyl of ZBG modified. After the HDAC1 enzyme activity test, **3j** was found to be the optimal compound. Specifically, different raw material acids **1a–1i** and 4-(aminomethyl)benzoic acid were coupled in the presence of *O*-(benzotriazol-1-yl)-*N*,*N*,*N*′,*N*′-tetramethyluronium-hexafluorophosphate (HBTU) to obtain key intermediates **2a–2i**. The key intermediates **2a–2i** are further condensed in the presence of HBTU with excess 1,2-phenylenediamine, pyridine-3,4-diamine, or 4-fluorobenzene-1,2-diamine to obtain target compounds **3a–3o,** respectively. All target compounds were fully characterized by MS (mass spectrometry) and ^{1}H nuclear magnetic resonance (NMR) spectra.

These target compounds in this study were initially tested for inhibition of recombinant human HDAC1 since our work and that of others have clearly shown that HDAC1 is widely implicated in both transcriptional repression and chromatin remodeling.[22–24]

First, we synthesized compounds **3a–3 g** (►**Table 1**) and discussed the effect of different fragments in the cap region on the inhibitory activity of HDAC1. It was found that when the indole fragment was inserted, compound **3 g** (HDAC1 $IC_{50} = 0.803$ μmol/L) had better enzyme inhibitory activity on HDAC1 than the positive control drug chidamide (HDAC1 $IC_{50} = 1.280$ μmol/L). When other fragments like quinoline, naphthalene, and thiazole are connected, the inhibitory activity of HDAC1 is much lower than that of indole fragment derivatives. Next, compounds **3h–3o** were synthesized with different substituents inserting into the 5-position of indole and the *o*-aminophenyl group of ZBG modified (►**Table 1**). The HDAC1 inhibitory activity was best when ZBG is 1,2-phenylenediamine, rather than pyridine-3,4-diamine or 4-fluorobenzene-1,2-diamine, with the IC_{50} value of **3 g** < **3h** < **3i**, **3j** < **3k** < **3l**, **3m** < **3n** < **3o**. Compound **3j** with the 5-position substituent of indole being fluorine (HDAC1 $IC_{50} = 0.330$ μmol/L) has the best inhibitory activity against HDAC1, which exceeds the positive control drug MS-275 (HDAC1 $IC_{50} = 0.668$ μmol/L).

Encouraged by its HDAC1 inhibitory profile, the preferred compound **3j** was progressed to *in vitro* antiproliferative activity assay against a panel of human cancer cells (PC-3, HCT-116, HUT-78, Jurkat E6–1, A549, Colo205, and MCF-7) and human fetal lung fibroblast normal cell lines MRC-5 using CCK-8 assay. Data from ►**Table 2** demonstrated that **3j** exhibited broad antiproliferative activities in most tested cancer cell lines with low IC_{50} values, ranging from 0.0088 μmol/L (HUT-78) to 1.248 μmol/L (A549). Notably, compound **3j** showed significant growth inhibition with IC_{50} values of 0.1914, 0.09903, 0.0088, and 0.128 μmol/L against PC-3, HCT-116, HUT-78, and Jurkat e6–1 cells, which were superior to

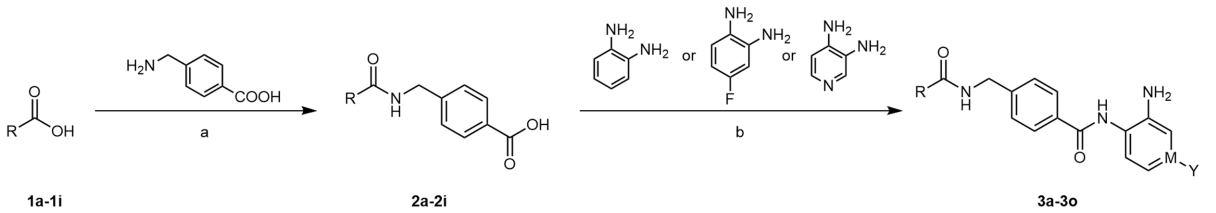

Compound	R	M	Y
3a	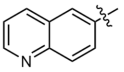	CH	-
3b	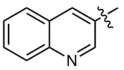	CH	-
3c	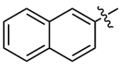	CH	-
3d	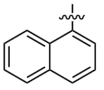	CH	-
3e	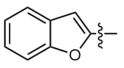	CH	-
3f	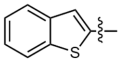	CH	-
3g	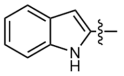	CH	-

Compound	R	M	Y
3h	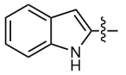	C	F
3i	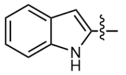	N	-
3j	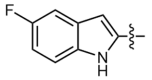	CH	-
3k	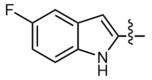	C	F
3l	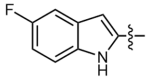	N	-
3m	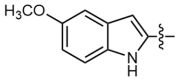	CH	-
3n	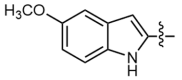	C	F
3o	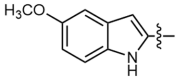	N	-

Scheme 1 Synthesis of compounds **3a–3o**. Reagent and conditions: (a) i. HBTU, TEA, r.t., NaOH (aq), 4 hours, CH_3CN; ii. HCl (aq), pH = 5–6; (b) HBTU, TEA, DMF, r.t., 6 hours. HBTU, *O*-(benzotriazol-1-yl)-*N*,*N*,*N*′,*N*′ -tetramethyluronium-hexafluorophosphate.

MS-275 (IC_{50} values were 0.502, 0.3674, 0.5281, and 0.5614 μmol/L, respectively). Furthermore, the tested compound **3j** showed weak inhibitory activity against MRC-5 cell lines ($IC_{50} > 100$ μmol/L), which indicated their differential growth inhibitory activities toward human cancer cells with desirable selectivity over human normal cell MRC-5.

To evaluate the potency and subtype selectivity, compound **3j** was further chosen for *in vitro* assays against part of HDAC enzyme subtypes, including HDAC enzymes of class I (HDAC1, 2, and 8) and class IIb (HDAC6). As the result shown in ►**Table 3**, compound **3j** showed good selectivity against HDAC1 over HDAC2 (IC_{50} values against HDAC2 was 8.4 μmol/L), and was inactive against both HDAC8 ($IC_{50} > 10$ μmol/L) and HDAC6 ($IC_{50} > 10$ μmol/L). *In vitro* cardiovascular safety was assessed in a patch-clamp hERG K^+ channel screen (►**Table 3**). Our data showed that compound **3j** was inactive in hERG binding assay with a IC_{50} >30 μmol/L (reducing incidence of QT interval prolongation). As is apparent from the data in ►**Table 3**, compound **3j** exhibited low toxicity to ICR mice with maximum tolerance dose value over 3,000 mg/kg by oral administration.

To gain insights into the possible interactions of **3j** with the active site of HDAC1 (PDB code: 4BKX), the molecular docking was performed. Consistent with the biochemical results, compound **3j** could bind well with HDAC1 (►**Fig. 3**). The amino group of compound **3j** could chelate the Zn^{2+} very well (1.94 Å to the nitrogen atom in aniline). Besides, two amino groups of amides formed two hydrogen-bonding interaction with ASP-99 and GLY-149, respectively. The benzene ring in the middle formed π–π stacking with PHE150 and HIE178. Collectively, the predicted molecular docking analysis further supports the experimental results that compound **3j** has tight contacts with HDAC1.

Meanwhile, the PK parameters of compound **3j** were measured in male Sprague–Dawley (SD) rats after single intravenous (iv; 5 mg/kg) and oral (po; 25 mg/kg) administration. When SD rats were administrated with **3j** (25 mg/kg, po), and a C_{max} of 1,950.7 ng/mL was obtained at 1.50 hours.

Table 1 Human HDAC1 enzyme inhibitory activities of all target compounds

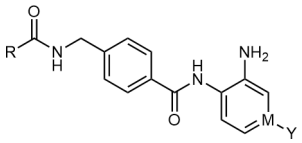

Compound	R	M	Y	HDAC1 IC_{50} (μmol/L)
3a	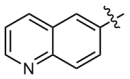	CH	–	9.401
3b	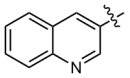	CH	–	11.67
3c	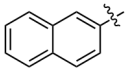	CH	–	12.21
3d	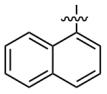	CH	–	18.43
3e	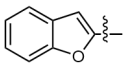	CH	–	5.432
3f	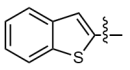	CH	–	4.298
3 g	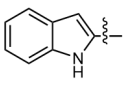	CH	–	0.803
3h	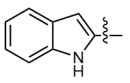	C	F	4.211
3i	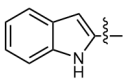	N	–	9.017
3j	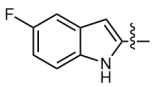	CH	–	0.330
3k	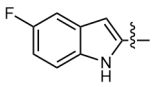	C	F	3.647
3l	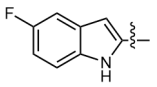	N	–	10.54

(*Continued*)

Table 1 (*Continued*)

Compound	R	M	Y	HDAC1 IC_{50} (μmol/L)
3m	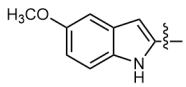	CH	–	0.553
3n	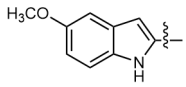	C	F	4.298
3o	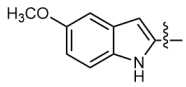	N	–	6.50
MS-275				0.668
Chidamide				1.280

Abbreviation: HDAC1, histone deacetylase 1.

Table 2 The antiproliferative activities of compound 3j and entinostat (MS-275)

Compound	IC_{50} (μmol/L)							
	PC-3	HCT-116	Hut-78	Jurkat E6–1	A549	Colo205	MCF-7	MRC-5
3j	0.1914	0.09903	0.0088	0.128	1.248	0.451	1.021	>100
MS-275	0.502	0.3674	0.5281	0.5614	2.278	1.09	2.718	>100

Table 3 IC_{50} value for the inhibition of HDAC enzyme subtypes, automated patch-clamp assay for hERG activity, and the MTD value in ICR mice

Compound	IC_{50} (μmol/L)				hERG IC_{50} (μmol/L)[a]	MTD (mg/kg)
	HDAC1	HDAC2	HDAC6	HDAC8		
3j	0.33	8.4	>10	>10	>30	>3,000

Abbreviations: HDAC, histone deacetylase; MTD, maximum tolerance dose.
[a]hERG patch clamp screen was performed as described in Dubin et al.[25] IC_{50} values represent the concentration to inhibit 50% of hERG current. Numbers represent IC_{50} values generated from 3-point concentration response relationships in duplicate.

The compound was well cleared (CL = 2.34 L/h/kg) in rats, and the elimination half-life was 4.38 hours. Compound **3j** was also well distributed (Vz = 14.64 L/kg) and had a moderate oral bioavailability (F = 29.5%) in rats (►**Table 4**).

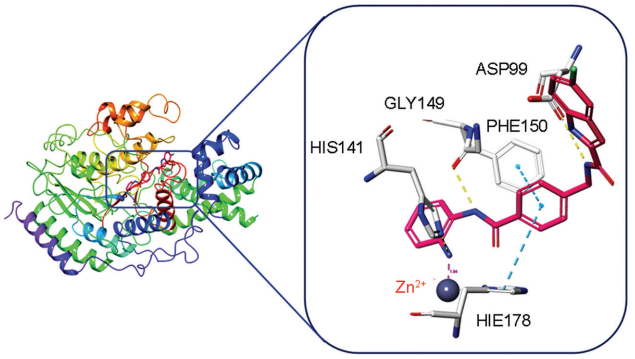

Fig. 3 Predicted binding modes of compound **3j** (carbon in pink) with HDAC1 (PDB entry: 4BKX). Hydrogen bonds are depicted as yellow lines and π–π stacking are depicted as cyan lines.

The antitumor activity of compound **3j** in a mouse xenograft model (PC-3, prostate cancer) was further assessed using MS-275 as a positive control. The mice were given daily intragastric (ig) doses of 12.5, 25, and 50 mg/kg of

Table 4 Pharmacokinetic parameters of compound 3j

Parameter	25 mg/kg (po)	5 mg/kg (iv)
$AUC_{(0\text{-}t)}$ (ng/mL × h)	10,567.0	7,160.2
$AUC_{(0\text{-}\infty)}$ (ng/mL × h)	10,741.8	7,160.8
$MRT_{(0\text{-}t)}$ (h)	4.61	0.96
V_Z (L/kg)	14.64	0.93
CL (L/h/kg)	2.34	0.71
$t_{1/2}$ (h)	4.38	0.91
T_{max} (h)	1.50	
C_{max} (ng/mL)	1,950.7	7,455.3
F (%)	29.5	

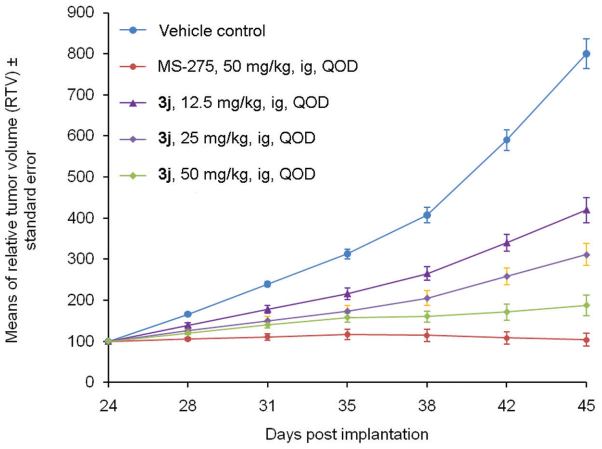

Fig. 4 The RTV curve of each group of animals during the administration period. RTV was measured by calculating the ratio of $V_t/V_{initial}$, where V_t is the tumor volume at each measurement, and $V_{initial}$ is the tumor volume measured at the time of group administration. RTV, relative tumor volume.

compound **3j** for 21 days, then the relative tumor volume was recorded from day 24 to day 45 since the treatment (►**Fig. 4**). Our data suggested that the mice were tolerant at a dose of 50 mg/kg (ig) and the ratio of tumor volume (day 45) in treated versus control mice (T/C) was 23.38%. In the same dose group of MS-275, the T/C was 12.97%. The tested mice did not experience significant weight loss (data not shown). It can be seen that compound **3j** shows significant antitumor activity in the PC-3 tumor xenograft model *in vivo*, though not as potent as positive control entinostat (MS-275).

Conclusion

In summary, we designed and synthesized a series of new benzamide HDAC1 inhibitors based on the structure of chidamide and MS-275. Our preliminary SAR analysis showed that the introduction of indole fragments into the cap region had a better inhibitory activity on HDAC1 than chidamide. The most promising compound **3j** exhibited more potent activities in both HDAC1 enzymatic inhibitory activity and cellular antiproliferative activity in comparation to MS-275. Compound **3j** did not possess observed effects on normal human cells and the hERG potassium channel, and selectively inhibited HDAC1 over the other tested HDAC isoforms. Molecular docking suggested good binding of **3j** with HDAC1. Meanwhile, compound **3j** had good PK properties and significantly inhibited tumor growth in an PC-3 prostate cancer mouse xenograft model study. It can be seen that compound **3j** is a safe and effective HDAC1 inhibitor and may be a potential compound for further cancer treatment.

Experimental Section

Instruments and Reagents

All starting materials were obtained from commercial sources and were analytically pure. The ^{1}H NMR spectra were recorded on Bruker Avance 400 or 600 spectrometers (Bruker Company, Germany) using TMS as an internal standard and DMSO-d_6 as solvents. The mass spectra were recorded on an Esquire 3000 LC-MS mass spectrometer. The melting point was measured with a WRS-2A microcomputer melting point apparatus (Shanghai Yidian Physical Optical Instrument Co., Ltd.) without the calibration of thermometer. Absorbance was measured using a SpectraMax M5 Microplate Reader (Molecular Devices). Thin-layer chromatography analyses were performed on silica gel plates GF254 (Qingdao Haiyang Chemical, China). Column chromatography separations were performed on silica gel 200–300 mesh.

General Synthetic Procedure of 2a–2i

Acid **1a–1i** (34.65 mmol) and HBTU (40.88 mmol) were added into acetonitrile (20 mL) and stirred evenly to form a paste. After 20 minutes, triethylamine (TEA) (87.31 mmol) was added. The reaction solution was cooled, and continued to stir at room temperature (r.t.) for 2 hours. To the reaction solution was added dropwise a solution of *p*-methylaminobenzoic acid (5.34 g, 35.34 mmol) in aqueous NaOH solution (1.41 g, 35.34 mmol in 20 mL of water). The resulting mixture was stirred at r.t. overnight. The next day, the ice water was cooled, filtered out the insoluble impurities, and the pH value was adjusted to 5–6 with dilute hydrochloric acid to precipitate a solid. The suspension was stirred for 3 hours and filtered to obtain a condensation product, which was washed with water, and filtered to obtain the intermediates **2a–2i**.

General Synthetic Procedure of 3a–3o

A mixture of intermediates **2a–2i** (7.02 mmol) and HBTU (7.37 mmol) in 10 mL of DMF was stirred uniformly for 15 minutes followed by the addition of TEA (33.34 mmol), and the mixture was stirred at r.t. for 2 hours. Then, benzene-1,2-diamine, 4-fluorobenzene-1,2-diamine or pyridine-3,4-diamine (8.35 mmol) was added. The reaction solution was stirred at r.t. overnight, then slowly dropped into 50 mL of water to precipitate a solid. The suspension was stirred for 3 hours and filtered to obtain the target compounds **3a–3o**.

***N*-(4-((2-aminophenyl)carbamoyl)benzyl)quinoline-6-carboxamide (3a)**: mp 192.0–192.9°C. ESI-MS (*m*/*z*): calcd. for $C_{24}H_{20}N_4O_2$ $[M+H]^+$ 397.1586; found 397.10. ^{1}H NMR (600 MHz, DMSO-d_6) δ 9.64 (s, 1H), 9.39 (t, J = 6.0 Hz, 1H), 9.00 (dd, J = 4.2, 1.7 Hz, 1H), 8.59 (d, J = 2.0 Hz, 1H), 8.50 (dd, J = 8.3, 1.8 Hz, 1H), 8.24 (dd, J = 8.8, 2.0 Hz, 1H), 8.12 (d, J = 8.7 Hz, 1H), 7.97 (d, J = 8.0 Hz, 2H), 7.63 (dd, J = 8.3, 4.2 Hz, 1H), 7.50 (d, J = 8.0 Hz, 2H), 7.18 (d, J = 7.8 Hz, 1H), 6.98 (td, J = 7.6, 1.5 Hz, 1H), 6.79 (dd, J = 8.0, 1.4 Hz, 1H), 6.60 (td, J = 7.4, 1.4 Hz, 1H), 4.90 (s, 2H), 4.63 (d, J = 5.9 Hz, 2H).

***N*-(4-((2-aminophenyl)carbamoyl)benzyl)quinoline-3-carboxamide (3b)**: mp 191.9–196.5°C. ESI-MS (*m*/*z*): calcd. for $C_{24}H_{20}N_4O_2$ $[M+H]^+$ 397.1586; found 397.10. ^{1}H NMR (600 MHz, DMSO-d_6) δ 9.65 (s, 1H), 9.49 (t, J = 6.0 Hz, 1H), 9.35 (d, J = 2.3 Hz, 1H), 8.91 (d, J = 2.4 Hz, 1H), 8.12 (t, J = 8.8 Hz, 2H), 7.98 (d, J = 7.8 Hz, 2H), 7.89 (ddd, J = 8.3, 6.8, 1.5 Hz, 1H), 7.73–7.70 (m, 1H), 7.52 (d, J = 7.9 Hz, 2H), 7.18 (d, J = 7.8 Hz, 1H), 6.98 (td, J = 7.6, 1.5 Hz, 1H), 6.80–6.78 (m,

1H), 6.61 (t, $J = 7.1$ Hz, 1H), 4.90 (s, 2H), 4.65 (d, $J = 5.9$ Hz, 2H).

***N*-(4-((2-aminophenyl)carbamoyl)benzyl)-2-naphthamide (3c)**: mp 193.1–195.6°C. ESI-MS (m/z): calcd. for $C_{25}H_{21}N_3O_2$ $[M+H]^+$ 396.1634; found 396.1731. ^{1}H NMR (400 M Hz, DMSO-d_6) δ 9.56 (s, 1H), 9.22 (t, $J = 6.0$ Hz, 1H), 8.52 (s, 1H), 8.02 (m, 6H), 7.62 (m, 2H), 7.49 (d, $J = 8.0$ Hz, 2H), 7.18 (d, $J = 7.6$ Hz, 1H), 6.97 (t, $J = 7.2$ Hz, 1H), 6.78 (d, $J = 8.0$ Hz, 1H), 6.60 (t, $J = 7.2$ Hz, 1H), 4.84 (s, 2H), 4.61 (d, $J = 6.0$ Hz, 2H).

***N*-(4-((2-aminophenyl)carbamoyl)benzyl)-1-naphthamide (3d)**: mp 241.6–243.3°C, ESI-MS (m/z): calcd. for $C_{25}H_{21}N_3O_2$ $[M+H]^+$ 396.1634; found 396.1729. ^{1}H NMR (400 M Hz, DMSO-d_6) δ 9.61 (s, 1H), 9.11 (t, $J = 6.0$ Hz, 1H), 8.22 (t, $J = 5.2$ Hz, 1H), 8.00 (m, 4H), 7.67 (dd, $J = 1.2$ Hz, 8.0 Hz, 1H), 7.57 (m, 5H), 7.19 (d, $J = 7.2$ Hz, 1H), 6.98 (dt, $J = 1.2$ Hz, 8.0 Hz, 1H), 6.80 (dd, $J = 1.2$ Hz, 8.0 Hz, 1H), 6.62 (dt, $J = 1.2$ Hz, 8.0 Hz, 1H), 4.84 (s, 2H), 4.62 (d, $J = 6.0$ Hz, 2H).

***N*-(4-((2-aminophenyl)carbamoyl)benzyl)benzofuran-2-carboxamide (3e)**: mp 159.2–160.4°C. ESI-MS (m/z): calcd. for $C_{23}H_{19}N_3O_3$ $[M+H]^+$ 386.4230; found 386.9851. ^{1}H NMR (400 M Hz, DMSO-d_6) δ 9.58 (s, 1H), 9.31 (s, 1H), 7.91 (m, 2H), 7.65 (d, $J = 8.0$ Hz, 1H), 7.57 (d, $J = 2.4$ Hz, 1H), 7.45 (m, 4H), 7.34 (t, $J = 7.6$ Hz, 1H), 7.16 (d, $J = 7.6$ Hz, 1H), 6.95 (dt, $J = 1.2$ Hz, 8.0 Hz, 1H), 6.78 (d, $J = 8.0$ Hz, 1H), 6.59 (dt, $J = 1.2$ Hz, 8.0 Hz, 1H), 4.81 (s, 2H), 4.54 (d, $J = 7.2$ Hz, 2H).

***N*-(4-((2-aminophenyl)carbamoyl)benzyl)benzo[*b*]thiophene-2-carboxamide (3f):** mp 159.3–162.0°C. ESI-MS (m/z): calcd. for $C_{23}H_{19}N_3O_2S$ $[M+H]^+$ 402.1198; found 402.1301. ^{1}H NMR (400 M Hz, DMSO-d_6) δ 9.65 (s, 1H), 9.44 (t, $J = 8.0$ Hz, 1H), 8.17 (s, 1H), 8.04 (d, $J = 8.0$ Hz, 2H), 7.97 (d, $J = 8.0$ Hz, 2H), 7.45 (m, 4H), 7.17 (d, $J = 8.0$ Hz, 1H), 6.97 (t, $J = 8.0$ Hz, 1H), 6.78 (d, $J = 8.0$ Hz, 1H), 6.60 (t, $J = 8.0$ Hz, 1H), 4.90 (s, 2H), 4.58 (d, $J = 8.0$ Hz, 2H).

***N*-(4-((2-aminophenyl)carbamoyl)benzyl)-1*H*-indole-2-carboxamide (3 g):** mp 233.7–234.7°C ESI-MS (m/z): calcd. for $C_{23}H_{20}N_4O_2$ $[M+H]^+$ 386.1586; found 385.1761. ^{1}H NMR (400 M Hz, DMSO-d_6) δ 11.47 (s, 1H), 9.51 (s, 1H), 8.98 (t, $J = 6.0$ Hz, 1H), 7.89 (d, $J = 8.0$ Hz, 2H), 7.46 (d, $J = 8.0$ Hz, 1H), 7.41 (m, 4H), 7.13 (m, 3H), 6.99 (dt, $J = 0.8$ Hz, 8.0 Hz, 1H), 6.73 (dd, $J = 1.2$ Hz, 7.6 Hz, 1H), 6.55 (dt, $J = 1.2$ Hz, 7.6 Hz, 1H), 4.77 (s, 2H), 4.53 (d, $J = 6.4$ Hz, 2H).

***N*-(4-((2-amino-4-fluorophenyl)carbamoyl)benzyl)-1*H*-indole-2-carboxamide (3h)**: mp 224.5–225.5°C. ESI-MS (m/z): calcd. for $C_{23}H_{19}FN_4O_2$ $[M+H]^+$ 403.1492; found 403.1524. ^{1}H NMR (400 M Hz, DMSO-d_6) δ 11.47 (s, 1H), 9.45 (s, 1H), 8.98 (t, $J = 6.0$ Hz, 1H), 7.89 (d, $J = 8.0$ Hz, 2H), 7.57 (d, $J = 8.0$ Hz, 1H), 7.40 (m, 3H), 7.13 (m, 2H), 7.06 (dt, $J = 2.4$ Hz, 8.8 Hz, 1H), 6.98 (dt, $J = 0.8$ Hz, 8.0 Hz, 1H), 6.49 (dd, $J = 2.8$ Hz, 11.2 Hz, 1H), 6.30 (dt, $J = 2.8$ Hz, 8.8 Hz, 1H), 5.09 (s, 2H), 4.53 (d, $J = 6.0$ Hz, 2H).

***N*-(4-((3-aminopyridin-4-yl)carbamoyl)benzyl)-1*H*-indole-2-carboxamide (3i):** mp 210.6–213.6°C. ESI-MS (m/z): calcd. for $C_{22}H_{19}N_5O_2$ $[M+H]^+$ 386.1539; found 386.1643. ^{1}H NMR (400 M Hz, DMSO-d_6) δ 11.47 (s, 1H), 9.60 (s, 1H), 8.99 (t, $J = 6.0$ Hz, 1H), 8.04 (s, 1H), 7.88 (d, $J = 8.0$ Hz, 2H), 7.74 (d, $J = 5.2$ Hz, 1H), 7.56 (d, $J = 8.0$ Hz, 1H), 7.40 (m, 4H), 7.13 (t, $J = 8.0$ Hz, 2H), 6.98 (t, $J = 7.2$ Hz, 1H), 5.05 (s, 2H), 4.53 (d, $J = 6.4$ Hz, 2H).

***N*-(4-((2-aminophenyl)carbamoyl)benzyl)-5-fluoro-1*H*-indole-2-carboxamide (3j):** mp 244.7–246.6°C. ESI-MS (m/z): calcd. for $C_{23}H_{19}FN_4O_2$ $[M+H]^+$ 403.1492; found 403.1586. ^{1}H NMR (400 M Hz, DMSO-d_6) δ 11.65 (s, 1H), 9.56 (s, 1H), 9.08 (t, $J = 6.0$ Hz, 1H), 7.95 (d, $J = 8.4$ Hz, 2H), 7.47 (m, 4H), 7.18 (m, 2H), 7.05 (dd, $J = 2.8$ Hz, 8.4 Hz, 1H), 6.95 (dt, $J = 1.2$ Hz, 7.6 Hz, 1H), 6.77 (dd, $J = 0.8$ Hz, 8.0 Hz, 1H), 6.59 (dt, $J = 1.2$ Hz, 7.6 Hz, 1H), 4.83 (s, 2H), 4.58 (d, $J = 6.0$ Hz, 2H).

***N*-(4-((2-amino-4-fluorophenyl)carbamoyl)benzyl)-5-fluoro-1*H*-indole-2-carboxamide (3k)**: mp > 250°C. ESI-MS (m/z): calcd. for $C_{23}H_{18}F_2N_4O_2$ $[M+H]^+$ 421.1398; found 421.1476. ^{1}H NMR (400 M Hz, DMSO-d_6) δ 11.63 (s, 1H), 9.51 (s, 1H), 9.09 (t, $J = 5.6$ Hz, 1H), 7.94 (d, $J = 8.0$ Hz, 2H), 7.43 (m, 4H), 7.17 (s, 1H), 7.04 (dt, $J = 2.4$ Hz, 9.6 Hz, 1H), 6.35 (dt, $J = 2.0$ Hz, 8.4 Hz, 1H), 6.55 (dd, $J = 2.8$ Hz, 10.8 Hz, 1H), 6.35 (dt, $J = 2.8$ Hz, 8.4 Hz, 1H), 5.13 (s, 2H), 4.57 (d, $J = 6.0$ Hz, 2H).

***N*-(4-((3-aminopyridin-4-yl)carbamoyl)benzyl)-5-fluoro-1*H*-indole-2-carboxamide (3l):** mp > 250°C. ESI-MS (m/z): calcd. for $C_{22}H_{18}FN_5O_2$ $[M+H]^+$ 404.1445; found 404.1524. ^{1}H NMR (400 M Hz, DMSO-d_6) δ 11.65 (s, 1H), 9.65 (s, 1H), 9.10 (t, $J = 6.0$ Hz, 1H), 8.10 (s, 1H), 7.94 (d, $J = 8.4$ Hz, 2H), 7.79 (d, $J = 5.2$ Hz, 1H), 7.47 (m, 5H), 7.18 (s, 1H), 7.04 (dt, $J = 1.2$ Hz, 9.6 Hz, 1H), 5.11 (s, 2H), 4.59 (d, $J = 6.0$ Hz, 2H).

***N*-(4-((2-aminophenyl)carbamoyl)benzyl)-5-methoxy-1*H*-indole-2-carboxamide (3m):** mp 231.3–233.0°C. ESI-MS (m/z): calcd. for $C_{24}H_{22}N_4O_3$ $[M+H]^+$ 415.1692; found 415.1769. ^{1}H NMR (400 M Hz, DMSO-d_6) δ 11.38 (s, 1H), 9.56 (s, 1H), 8.99 (t, $J = 6.0$ Hz, 1H), 7.95 (d, $J = 8.0$ Hz, 2H), 7.46 (d, $J = 8.0$ Hz, 2H), 7.33 (d, $J = 8.8$ Hz, 1H), 7.18 (d, $J = 7.6$ Hz, 1H), 7.10 (m, 2H), 6.97 (dt, $J = 1.2$ Hz, 7.6 Hz, 1H), 6.85 (dd, $J = 2.4$ Hz, 8.8 Hz, 1H), 6.78 (dd, $J = 1.2$ Hz, 7.6 Hz, 1H), 6.60 (dt, $J = 1.2$ Hz, 7.6 Hz, 1H), 4.83 (s, 2H), 4.58 (d, $J = 6.0$ Hz, 2H), 3.77 (s, 3H).

***N*-(4-((2-amino-4-fluorophenyl)carbamoyl)benzyl)-5-methoxy-1*H*-indole-2-carboxamide (3n):** mp 226.9–227.2°C. ESI-MS (m/z): calcd. for $C_{24}H_{21}FN_4O_3$ $[M+H]^+$ 433.1598; found 433.1680. ^{1}H NMR (400 M Hz, DMSO-d_6) δ 11.38 (s, 1H), 9.50 (s, 1H), 8.98 (t, $J = 6.0$ Hz, 1H), 7.95 (d, $J = 8.4$ Hz, 2H), 7.45 (d, $J = 8.0$ Hz, 2H), 7.35 (s, 1H), 7.13 (m, 3H), 6.84 (dd, $J = 2.4$ Hz, 8.8 Hz, 1H), 6.55 (dd, $J = 3.2$ Hz, 11.2 Hz, 1H), 6.35 (td, $J = 2.8$ Hz, 8.4 Hz, 1H), 5.15 (s, 2H), 4.58 (d, $J = 6.0$ Hz, 2H), 3.77 (s, 3H).

***N*-(4-((3-aminopyridin-4-yl)carbamoyl)benzyl)-5-methoxy-1*H*-indole-2-carboxamide (3o):** mp 229.7–230.6°C. ESI-MS (m/z): calcd. for $C_{23}H_{21}N_5O_3$ $[M+H]^+$ 416.1644; found 416.1706. ^{1}H NMR (400 M Hz, DMSO-d_6) δ 11.38 (s, 1H), 9.65 (s, 1H), 8.99 (t, $J = 5.6$ Hz, 1H), 8.11 (s, 1H), 7.94 (d, $J = 8.4$ Hz, 2H), 7.80 (d, $J = 5.2$ Hz, 1H), 7.49 (d, $J = 8.4$ Hz, 2H), 7.43 (d, $J = 5.2$ Hz, 1H), 7.33 (d, $J = 8.8$ Hz, 1H), 7.10 (s, 2H), 6.85 (dd, $J = 2.0$ Hz, 6.8 Hz, 1H), 5.11 (s, 2H), 4.59 (d, $J = 6.0$ Hz, 2H), 3.77 (s, 3H).

In Vitro Testing of HDAC1, HDAC2, HDAC6, and HDAC8

A 500 µmol/L of the tested compound was diluted with fourfold serial dilution to 0 µmol/L with DMSO. Then, to the optiPlate-96 black microplates (Perkinelmer, Cat:

6005270) was added 11.5 µL assay buffer (BPS, Cat: 50031) and 2.5 µL of compounds with different diluted concentrations at r.t. For negative control and blank control wells, 11.5 µL assay buffer were added, respectively, and for positive control wells, 11.5 µL assay buffer and 2.5 µL MS-275 were added. All determinations were performed in duplicate. A 6 µL of human recombinant HDAC1 (BPS, Cat: 50051), human recombinant HDAC1 (BPS, Cat: 50062), or human recombinant HDAC6 (BPS, Cat: 50006) was added respectively to microplates and incubated for 10 minutes. Then, 2.5 µL BSA was added to each reaction well, followed by the addition of 2.5 µL HDAC substrate (BPS, Cat: 50037). The mixture was incubated at 37°C for 45 minutes, then added the stop solution (HDAC developer [BPS, Cat: 50030], 25 µL). After incubation at 25°C for 15 minutes, the fluorescence was measured on SpectraMax M5 (Molecular Devices) with an excitation wavelength of 360 nm and an emission wavelength of 460 nm.

A commercial HDAC8 fluorimetric drug discovery kit [Fluor de Lys(R)-HDAC8, BMLKI178] was used to perform HDAC8 activity assay according to the manufacturer's instructions. The enzyme was incubated for 90 minutes at 37°C, with a substrate concentration of 50 µmol/L and increasing concentrations of inhibitors. Measurement was performed as described for HDAC1/2/6.

The inhibition rates were calculated by the slope of the linear reaction process of each well as follows: %Inhibition $=$ (Mean (Max) $-$ Sample Signal)/(Mean (Max) $-$ Mean (Min)) $\times$ 100. The IC_{50} value of each compound's enzyme inhibitory activity was obtained by fitting the dose–response curve through GraphPad Prism 5 software.

CCK-8 Assay for Cell Proliferative Assessment

Cells were cultured in medium to log phase and then digested, centrifuged, and resuspended in fresh medium. Then, they were seeded into 96-well plates (Corning Costar, Cat: 3599, 104 cells/well) and incubated overnight at 37°C under 5% CO_2 atmosphere to make them reattach. Subsequently, cells were treated with the target compounds at decreasing concentrations (10 concentrations from a concentration of 100 µmol/L with threefold serial dilution) for another 24 hours. The absorbance values at 450 nm (optical density: 450) were recorded by SpectraMax M5 Microplate Reader (Molecular Devices). There are two repeated wells for each concentration. The IC_{50} value was defined as a concentration that caused 50% loss of cell viability, which was calculated by Origin 7.5 software.

Molecular Modeling Study

The docking study was conducted in Glide module of Schrodinger Maestro. PDB entry 4BKX was downloaded from Protein Data Bank for molecular docking. In Protein Preparation Wizard, the HDAC1 protein was prepared by the process of removing waters and adding hydrogens. The most important of resulting structure was refined in the force field of OPLS3 with the hydrogen only. Then, the Receptor Grid Preparation was defined according to the position of the zinc ion. Compound **3j** generated all possible combinations at the target pH 7.0 $\pm$ 2.0 in the force field of OPLS3 in LigPrep module. Ligand docking parameter used was set default. Molecular docking result was generated using PyMol (http://pymol.sourceforge.net/).

hERG Inhibitory Activity Assay

The whole-cell recordings were conducted using Automated Qpatch (Sophion).[26] Cells were voltage clamped at a holding potential of -80 mV. The hERG current was activated by depolarizing at $+20$ mV for 5 seconds, after which the voltage was taken back to -50 mV for 5 seconds to remove the inactivation and observe the deactivating hERG tail current. The voltage stimulation was applied per 15 seconds. Cells were treated with different concentrations of compound solutions (from low to high concentration) for 2 minutes and 10 µmol/L cisapride was applied at the end of perfusion of compound solution. Each concentration was tested on at least three cells.

Acute Toxicity Assay

ICR mice (18–22 g) were purchased from SLRC Laboratory Animal Inc., Shanghai, China. A total of 10 mice (five males, five females) were used in this study. Compound **3j** was administered orally to mice at a single dose of 3,000 mg/kg, respectively. Mouse death was monitored daily up to 14 days of treatment. All animals were euthanized and necropsied for gross lesion examination for possible damage to the heart, liver, and kidneys.

Pharmacokinetics Study

Compound **3j** was dissolved and vortexed in 5% DMSO, 10% Tween 80, and 75% physiological saline for a concentration of 0.2 mg/mL and 1 mg/mL. The male SD rats were housed in a room with controlled temperature and humidity and allowed free access to food and water. The rats were split into iv injection group (5 mg/kg) and ig administration group (25 mg/kg) before starting treatment. Rat blood was collected at indicated time points up to 12 hours, and plasma samples were analyzed using an Agilent 1200 HPLC system coupled with Agilent 6410B triple quadruple mass spectrometer. A solution of 0.05 N HCl in saline was used as the vehicle for both iv and po dosing.

In Vivo Antitumor Activity Assay

BALB/C nude mice were subcutaneously inoculated with PC-3 tumor cells to establish a PC-3 nude mouse xenograft model. After 24 days, the average tumor volume was $\sim$207 mm^3. Tumor-bearing mice were randomly divided into five groups: vehicle control, MS-275, and **3j** (12.5, 25, 50 mg/kg) groups. All groups were administered drugs (ig, 10 mL/kg) once every 2 days for 21 successive days. Mice in vehicle control were given blank solvent (3% ethanol, 10% HCl [pH 0.75], 20% solutol HS 15, 40% PEG400, and acetate buffer [pH 4.0]). Animal state was observed and recorded regularly every day; if the animal dies, the animal is grossly dissected, and the internal organs are visually observed for any abnormality and recorded. After 45 days, the animals were sacrificed, and the tumor mass was removed, weighed, and

photographed. Tumor weight and tumor inhibition rate were calculated. The tumor volume (V) was calculated as follows: $V = [\text{length (mm)} \times \text{width}^2 \text{ (mm}^2)]/2$.

Ethics Statement

The present study was approved by the animal ethics committee and abides by the relevant agreements of China State Institute of Pharmaceutical Industry, Shanghai, People's Republic of China.

Funding

This work was financially supported by the National Science and Technology Major Project (Grant No. 2018ZX09711002-002-009), the National Natural Science Foundation of China (Grant No. 81703358), and Science and Technology Commission of Shanghai Municipality (Grant No. 17431903900, 18QB1404200, and 21S11908000).

Conflict of Interest

The authors declare no conflicts of interests.

References

1 Bird A. Perceptions of epigenetics. Nature 2007;447 (7143):396–398
2 Jones RS. Epigenetics: reversing the 'irreversible'. Nature 2007; 450(7168):357–359
3 Zhang XH, Qin-Ma, Wu HP, et al. A review of progress in histone deacetylase 6 inhibitors research: structural specificity and functional diversity. J Med Chem 2021;64(03):1362–1391
4 Suvà ML, Riggi N, Bernstein BE. Epigenetic reprogramming in cancer. Science 2013;339(6127):1567–1570
5 Baylin SB, Ohm JE. Epigenetic gene silencing in cancer - a mechanism for early oncogenic pathway addiction? Nat Rev Cancer 2006;6(02):107–116
6 Hassig CA, Schreiber SL. Nuclear histone acetylases and deacetylases and transcriptional regulation: HATs off to HDACs. Curr Opin Chem Biol 1997;1(03):300–308
7 Zhang Q, Lu B, Li J. Design, synthesis and biological evaluation of 4-piperazinyl-containing chidamide derivatives as HDACs inhibitors. Bioorg Med Chem Lett 2017;27(14):3162–3166
8 Yuan H, Marmorstein R. Structural basis for sirtuin activity and inhibition. J Biol Chem 2012;287(51):42428–42435
9 Stengel KR, Hiebert SW. Class I HDACs affect DNA replication, repair, and chromatin structure: implications for cancer therapy. Antioxid Redox Signal 2015;23(01):51–65
10 Weichert W, Röske A, Gekeler V, et al. Histone deacetylases 1, 2 and 3 are highly expressed in prostate cancer and HDAC2 expression is associated with shorter PSA relapse time after radical prostatectomy. Br J Cancer 2008;98(03):604–610
11 Bonfils C, Hou Y, Besterman JM, et al. Specific inhibition of HDAC8 by antisenses leads to growth arrest and apoptosis of human cancer cells. Cancer Res 2005;65:424
12 Nakagawa M, Oda Y, Eguchi T, et al. Expression profile of class I histone deacetylases in human cancer tissues. Oncol Rep 2007;18 (04):769–774
13 HoTCS, Chan AHY, Ganesan A. Thirty years of HDAC inhibitors: 2020 insight and hindsight. J Med Chem 2020;63(21):12460–12484
14 Knipstein J, Gore L. Entinostat for treatment of solid tumors and hematologic malignancies. Expert Opin Investig Drugs 2011;20 (10):1455–1467
15 Lu X, Ning Z, Li Z, Cao H, Wang X. Development of chidamide for peripheral T-cell lymphoma, the first orphan drug approved in China. Intractable Rare Dis Res 2016;5(03):185–191
16 Zhang Y, Feng J, Jia Y, et al. Design, synthesis and primary activity assay of tripeptidomimetics as histone deacetylase inhibitors with linear linker and branched cap group. Eur J Med Chem 2011;46(11):5387–5397
17 Methot JL, Chakravarty PK, Chenard M, et al. Exploration of the internal cavity of histone deacetylase (HDAC) with selective HDAC1/HDAC2 inhibitors (SHI-1:2). Bioorg Med Chem Lett 2008;18(03):973–978
18 Dai Y, Guo Y, Curtin ML, et al. A novel series of histone deacetylase inhibitors incorporating hetero aromatic ring systems as connection units. Bioorg Med Chem Lett 2003;13(21):3817–3820
19 Singh A, Chang TY, Kaur N, et al. CAP rigidification of MS-275 and chidamide leads to enhanced antiproliferative effects mediated through HDAC1, 2 and tubulin polymerization inhibition. Eur J Med Chem 2021;215:113169
20 Chen T, Jiang H, Zhou J, et al. Synthesis of N-substituted benzamide derivatives and their evaluation as antitumor agents. Med Chem 2020;16(04):555–562
21 Paquin I, Raeppel S, Leit S, et al. Design and synthesis of 4-[(s-triazin-2-ylamino)methyl]-N-(2-aminophenyl)-benzamides and their analogues as a novel class of histone deacetylase inhibitors. Bioorg Med Chem Lett 2008;18(03):1067–1071
22 Zhang Z, Zhang Q, Zhang H, et al. Discovery of quinazolinyl-containing benzamides derivatives as novel HDAC1 inhibitors with in vitro and in vivo antitumor activities. Bioorg Chem 2021;117:105407
23 Willis-Martinez D, Richards HW, Timchenko NA, Medrano EE. Role of HDAC1 in senescence, aging, and cancer. Exp Gerontol 2010;45(04):279–285
24 Kawai H, Li H, Avraham S, Jiang S, Avraham HK. Overexpression of histone deacetylase HDAC1 modulates breast cancer progression by negative regulation of estrogen receptor alpha. Int J Cancer 2003;107(03):353–358
25 Dubin AE, Nasser N, Rohrbacher J, et al. Identifying modulators of hERG channel activity using the PatchXpress planar patch clamp. J Biomol Screen 2005;10(02):168–181
26 Kutchinsky J, Friis S, Asmild M, et al. Characterization of potassium channel modulators with QPatch automated patch-clamp technology: system characteristics and performance. Assay Drug Dev Technol 2003;1(05):685–693